https://doi.org/10.1007/s41230-025-4253-4

Investigating inclusions and mechanical properties of 1060 aluminum by salt fluxes refining

Jing-feng Wang[1, 2], Yao-heng Qiu[1], *Chao-yi Chen[1], **Lin-zhu Wang[1, 3], and Jun-qi Li[1]

1. School of Materials and Metallurgy, Guizhou University, Guiyang 550025, China

2. Zhengzhou Railway Vocational and Technical College, Zhengzhou 450000, China

3. Guizhou Provincial University Key Laboratory of High Performance Battery Materials, Guizhou University, Guiyang 550025, China

Abstract: In the casting process of 1060 industrial pure aluminum, the inclusions in the aluminum melt significantly affect the product quality. In this study, the influence of refining temperature and the composition of salt fluxes on the purification effect and mechanical properties of aluminum melt was investigated. The results indicate that lower refining temperatures and modified salt fluxes can effectively enhance the cleanliness of the aluminum melt. As the refining temperature increases, the large inclusions gradually increase. The addition of 16wt.% Na_3AlF_6 can dissolve and break up Al_2O_3 inclusions, facilitating the separation of the aluminum melt and aluminum slag. The addition of 16wt.% Na_3AlF_6 and 2wt.% $CaCO_3$ to the basic salt fluxes enables gas refinement, thereby further improving the cleanliness of the aluminum melt. Under the refining condition of 37wt.% NaCl-47wt.% KCl-16wt.% Na_3AlF_3-2wt.% $CaCO_3$ at 740 °C, better cleanliness and mechanical properties were obtained. The cleanliness and yield strength are approximately 99.99928% and 71.46 MPa, respectively. This work can offer valuable reference and theoretical insights for future research.

Keywords: 1060 aluminum; purification; inclusions; mechanical properties

CLC numbers: TG146.21 **Document code:** A **Article ID:** 1672-6421(2026)02-263-11

1 Introduction

1060 industrial pure aluminum has many advantages, such as easy processing, good corrosion resistance, excellent thermal conductivity, and low density[1]. In the refrigeration industry, due to its low cost, 1060 industrial pure aluminum is usually used as a substitute for copper in producing important components such as evaporators, condensers, capillaries, and dry filters. However, it is challenging to eliminate inclusions from the aluminum melt during the purification process, which negatively affects the quality of aluminum products. In 1060 industrial pure aluminum, inclusions disrupt the matrix's continuity and exhibit notable differences in properties compared to the matrix. Non-metallic inclusions serve as typical sources of fatigue cracks. The larger the inclusion size, the lower the fatigue strength[2, 3]. The inclusions in the matrix tend to cause stress concentrations at the sharp corners. They are common sources of material fractures and corrosion[4, 5]. Gao et al.[6] analyzed the "hard spots" in Al-Si-Cu alloy and found that the primary compositions of these "hard spots" are Al_2O_3 and trace amounts of Al_4C_3. The hardness of these spots ranged from 818.1 HV to 1,425.7 HV, which was over 14 times that of the aluminum alloy matrix. The formation of Al_4C_3 is caused by the introduction of carbon in the aluminum production process, such as the direct contact between graphite electrodes and molten salts in the electrolytic aluminum process, and the reaction between different organic compounds and melts during the processing[7, 8]. He et al.[9] investigated the impact of CO_2 generated through the anodic effect on the aluminum melt during the electrolysis process. They discovered that CO_2 reacted with the aluminum melt to form α-Al_2O_3 at high temperatures. Many studies have confirmed that over 99% of the inclusions in aluminum melts are Al_2O_3 inclusions, including various types such as

***Chao-yi Chen**

Male, born in 1977, Ph. D., Professor. His research interests mainly focus on new short-process metallurgical technologies, comprehensive utilization of metallurgical resources, and corrosion and protection.

E-mail: czchen@gzu.edu.cn

****Lin-zhu Wang**

E-mail: lzwang@gzu.edu.cn

Authors Jing-feng Wang and Yao-heng Qiu contributed equally to this work.

Received: 2024-11-22; Revised: 2025-01-13; Accepted: 2025-02-10

α-Al_2O_3, γ-Al_2O_3, and η-Al_2O_3. These inclusions can exhibit fragmented, granular, membranous, or plate-like shapes, with a wide size range from 1 nm to 1,000 μm[10, 11].

The preparation of high-quality 1060 aluminum ingots primarily depends on the purification level of the aluminum melt. Researchers have conducted extensive studies to efficiently remove inclusions from the melt[12-16]. Aluminum melt purification methods can be categorized into adsorption, non-adsorption, and composite purification. Among these methods, the salt fluxes method, as a kind of adsorption method, has become widely adopted in industrial production due to its advantages, such as ease operation, low cost, and high efficiency[17, 18]. It can effectively remove water from the solvent thoroughly, homogenize the components, and facilitate purification. Majidi et al.[18] investigated the impact of melting temperatures and adding salt fluxes on the refining process of A380 and A319 aluminum alloys. It is determined that the NaCl-KCl-Na_2SiF_6-CaF_2 flux is effective in removing inclusions from aluminum melt at 740 °C. Shi et al.[19] determined the optimal composition of fluoride in salt fluxes. They studied the interfacial tension between aluminum alloys and different fluoride salts added at 740 °C. The results indicated that adding KF, NaF, Na_3AlF_6, MgF_2, and AlF_3 reduced the interfacial tension between the aluminum alloy and the salt flux. The use of 0.5wt.% salt flux with 5wt.% KF in processing A356 aluminum alloy led to reduced levels of gas and inclusions. Tenorio et al.[20] studied the interaction between salt and inclusions during aluminum recycling, experimenting with equimolar NaCl and KCl. The results indicated that this mixture can facilitate the detachment of aluminum oxide layers. Wan et al.[10] identified the fluoride composition in salt fluxes used for aluminum recycling. Zhou et al.[21] used thermodynamic theory and surface renewal kinetics models to study the removal of inclusions in aluminum melts and the mechanism of aluminum grain refinement. They found that the tensile strength of specimens (castings) increased by 8.59% after treatment with salt fluxes. As for the detection of inclusions in aluminum and aluminum alloys, there are many available methods, including optical microscopy[22], ultrasound (both solid and liquid)[23], X-ray photography and tomography[24, 25], electromagnetic induction[26], fracture testing[27], vacuum testing[24], filtration and centrifugation[28], and chemical dissolution[29]. The primary limitation of these methods is their inability to rapidly determine the composition concentration, and size distribution of inclusions. In particular, the most popular detection methods, such as LiMCA (liquid metal cleanliness analyzer), are only capable of measuring the number and size distribution of inclusions larger than 10 μm in aluminum melts. PoDFA (Porous Disk Filtration Apparatus) is used to collect particles in molten metals onto the surface of fine ceramic filters, thereby assisting in the identification of inclusion types[30]. In this study, scanning electron microscopy was employed to observe inclusions in 1060 aluminum, and image analysis software was used for statistical analysis, effectively determining the composition, quantity, and size distribution of inclusions.

There are comprehensive reports on methods for removing inclusions from the melt and the failure behavior caused by inclusions[5, 16]. However, there is limited research regarding the factors that influence inclusions in aluminum melts and the mechanisms of formation, particularly concerning the analysis of typical inclusions morphology, quantity, and size. This study used the salt fluxes method to purify the 1060 industrial pure aluminum melt. The morphology, size, and quantity distribution of Al_2O_3 inclusions after purification at different temperatures were analyzed. The various salt fluxes compositions (including chlorides, cryolite, and calcium carbonate) and the forming mechanisms of inclusions were also investigated. Finally, mechanical properties were tested using the samples purified with modified salt fluxes at 740 °C.

2 Experimental

2.1 Materials

1060 aluminum obtained from Zunyi Hengjia Aluminum Co., Ltd. in China was used as the raw material. The chemical composition of the 1060 aluminum is presented in Table 1. The reagents used in the experiment were all analytical pure and were purchased from Sinopharm Chemical Reagent Co., Ltd.

Table 1: Chemical compositions of 1060 aluminum (wt.%)

Mn	Mg	Cu	Zn	Si	Fe	Ti	V	Al
0.002	0.004	0.001	0.0051	0.0470	0.166	0.0080	0.0011	Bal.

2.2 Experimental procedures

The process of salt fluxes synthesis is as follows. NaCl: KCl=1:1 (molar ratio) was mixed and placed in a corundum crucible. The mixture was heated to 800 °C in a muffle furnace, then naturally cooled. Afterward, the mixture was ground and sifted through a 200-mesh sieve to prepare the basic salt fluxes[31]. To obtain modified salt fluxes, varying amounts of Na_3AlF_6 and $CaCO_3$ were blended and ground together. Before introducing the salt fluxes into the aluminum melt, it was essential to thoroughly dry them at 300 °C for 4 h. This step can remove moisture and prevent the introduction of H_2O to the melt[21].

Refining process of aluminum melt was as follows: A 150 g aluminum ingot was placed in a corundum crucible, which was then placed inside a tube furnace, as illustrated in Fig. 1. The samples were heated to a specific temperature and maintained for 1 h to ensure the aluminum ingot completely melted. At different refining temperatures, salt fluxes with

varying compositions were wrapped in aluminum foil, introduced into the bottom of the melt, and vigorously stirred for 1 min using a molybdenum rod. The salt fluxes accounted for 1wt.% of the aluminum raw material. After removing the surface aluminum dross, the melt was cast into rod-shaped ingots. The remelted ingots were then cut into samples of 10 mm×10 mm×10 mm for subsequent analysis. After purification, the refined samples were compared with unrefined (blank) samples under the same conditions to evaluate the purification efficiency. All experiments were conducted under strictly controlled and consistent external conditions.

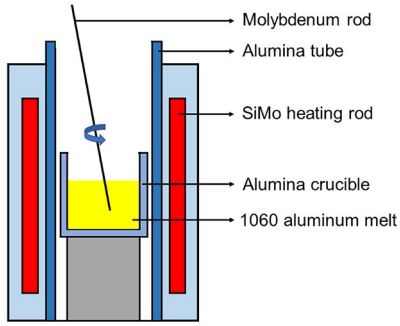

Fig. 1: Schematic diagram of melting

2.3 Analysis and characterization

The standard metallographic samples were cut from the equivalent positions in different aluminum ingots. The samples were ground, mechanically polished, and electrolytic polished. Subsequently, the polished samples were placed in an alcohol solution for ultrasonic cleaning. For electrolytic polishing, a 10% perchloric acid alcohol solution was used, the polished sample serving as the anode and stainless steel as the cathode. The polishing temperature was between 20–30 °C. Power voltage was 25 V, electrode spacing was 2 cm, and polish time ranged from 8–12 s. The characteristics of typical inclusions were analyzed using a scanning electron microscope (SEM, EM-30 plus, Coxem Co., Ltd.) under backscattering mode and energy dispersive X-ray spectroscopy (EDS, Ultim Max, Oxford Instruments, United Kingdom). In SEM testing, 50 consecutive images were taken at a magnification of 2000X for statistical analysis, with each photo measuring 100 μm×67.5 μm. The quantity and size of the inclusions were analyzed using the ImageJ image analysis software.

The melt cleanliness, denoted as D, was determined by the ratio of the total inclusion area S measured by ImageJ software in the SEM image to the total field of view area A in the statistical image. The total of view area A was calculated as the product of a single view area A_0 and the number of fields of view N.

$$D = 1 - \frac{S}{A} \tag{1}$$

$$A = N \times A_0 \tag{2}$$

To obtain the tensile strength, samples with a diameter of 9 mm and a length of 30 mm were tested on a tensile tester (IBTC-5000, Care Measurement & Control, China) at room temperature. Three samples were cut from each ingot and tested at a speed of 0.5 mm·min^{-1}.

3 Results and discussion

3.1 Effect of refining temperature on purification of aluminum melt

To determine the appropriate melt purification temperature, basic salt fluxes [NaCl:KCl=1:1 (molar ratio)] were used for the refining process. The typical morphology of inclusions in an aluminum melt at different refining temperatures is shown in Fig. 2. These inclusions typically exhibit small particles, films, and plates. EDS testing confirms that all these inclusions are mainly Al_2O_3, as shown in Fig. 3. α-Al_2O_3 and γ-Al_2O_3 coexist in the aluminum alloy, with the plate-like inclusions being γ-Al_2O_3 and the particle-like inclusions being α-Al_2O_3[24]. This is consistent with the studies of Impey[32] and Lee[33] et al. As the temperature increases, there is an increase in the number of Al_2O_3 inclusions which are found in small particles, along with a corresponding increase in pores.

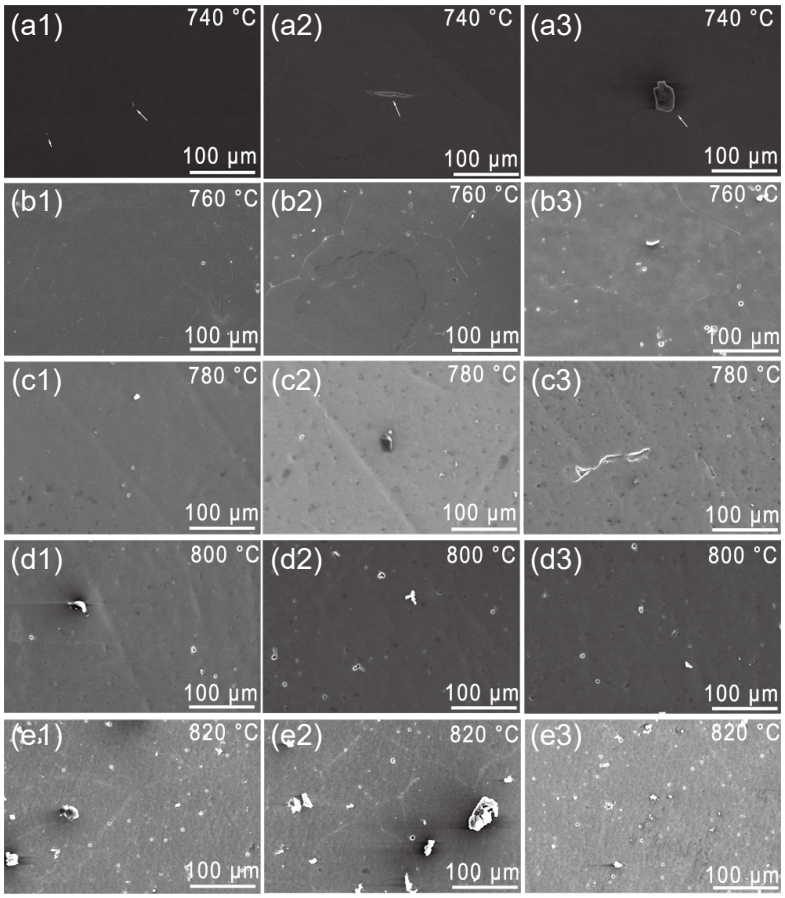

Fig. 2: Morphologies of inclusions in aluminum melt at different temperatures: (a1–a3) 740 °C; (b1–b3) 760 °C; (c1–c3) 780 °C; (d1–d3) 800 °C; (e1–e3) 820 °C

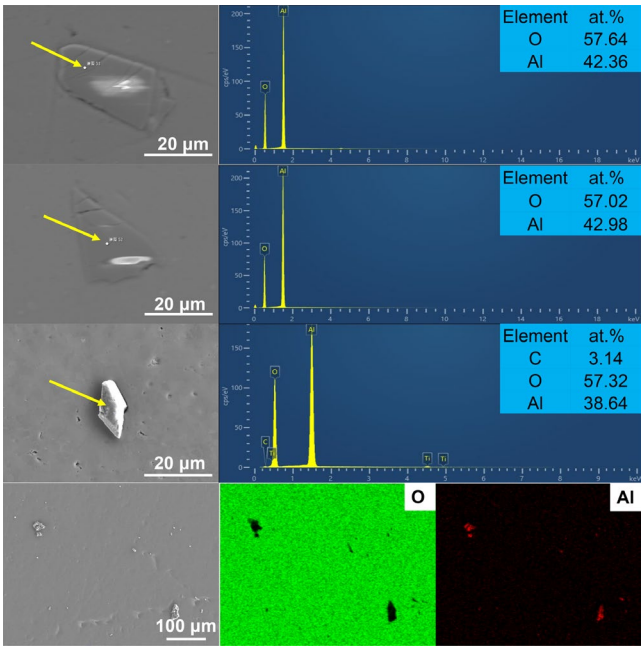

Fig. 3: SEM and EDS results of Al_2O_3 inclusions

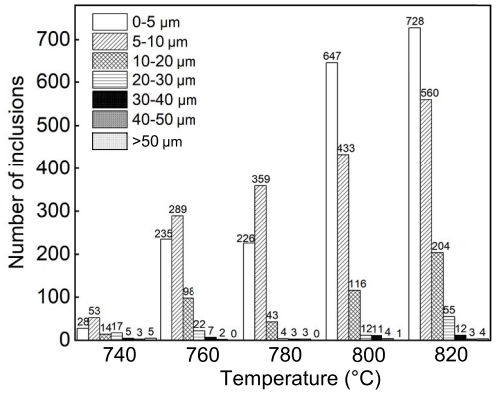

Fig. 4: Distribution of inclusion number and size at different purification temperatures

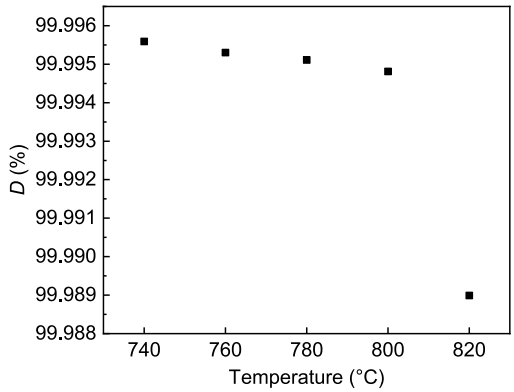

Fig. 5: Cleanliness (*D*) of aluminum melt at different purification temperatures

The size and number distribution of inclusions at different purification temperatures is presented in Fig. 4. As the purification temperature increases, the number of inclusions increases, especially within the 0–10 μm range. Furthermore, during the melting process at temperatures above 800 °C, the proportion of inclusions in the 0–5 μm size range is notably higher than that in other size ranges. When analyzing the size distribution of inclusions, it becomes evident that inclusions in the 0–10 μm size range consistently dominate in quantity compared to other size ranges. Conversely, inclusions larger than 30 μm are less common.

The results of melt cleanliness (*D*) in the aluminum melt are illustrated in Fig. 5. It is evident that cleanliness decreases as the temperature increases. Especially, at 820 °C, the aluminum melt exhibits the lowest cleanliness. A decrease in melt cleanliness is observed to occur concurrently with an increase in inclusion content, indicating a significant correlation between these factors. This trend is attributed to the increased number of inclusions generated during high-temperature melting.

The size and quantity distribution of inclusions, along with variations in cleanliness, were primarily influenced by alterations in the surface structure of Al_2O_3 in the melt[24, 34, 35]. During the casting process, Al_2O_3 particles can form inevitably[34]. With increasing temperature, the aluminum melt undergoes enhanced oxidation due to exposure to air. The surface structure of aluminum oxide in the melt is changed. Yu et al.[36] used synchronous thermal analysis technology to investigate the oxidation process of aluminum in a non-high-pressure air environment. The researchers also conducted phase analysis on the surface oxides of aluminum powder particles. Their findings suggested that γ-Al_2O_3 transformed into α-Al_2O_3 at 773 °C, and α-Al_2O_3 began to grow at 800 °C. Impey et al.[32] observed the melt's surface under melting conditions at 750 °C, and noted that γ-Al_2O_3 was broken and the nodular structure was formed by the oxidation of the aluminum melt which seeped out at the fracture site. This phenomenon suggested that during the transformation of γ-Al_2O_3 into α-Al_2O_3, its volume decreased by 24%. The tensile stress caused by volume changes broke the originally dense oxide film. The small-sized oxide film was immersed in the aluminum melt. The higher refining temperatures render the aluminum oxide layer on the melt's surface more fragile, causing it to submerge in the melt[32]. Consequently, as the exposed melt initiates oxidation, a new oxide layer forms and becomes entrained into the melt during production processes, leading to an increase in fine granular oxide inclusions. With increasing temperature, this oxidation intensifies, resulting in a significant rise in the number of alumina inclusions, predominantly in the 0–10 μm range. The proliferation of fine inclusions leads to a noticeable decrease in overall melt cleanliness, indicating that elevated temperatures not only enhance oxidation but also accelerate the dispersion and refinement of alumina inclusion surface structures within the 740–820 °C range.

The increase in porosity can be attributed to hydrogen absorption, melt oxidation, and the removal of transition elements from the melt, as shown in Fig. 2. Excess hydrogen in the melt forms pores with increasing temperature during the solidification process. Simultaneously, melt oxidation and the elimination of transition elements lead to increased pore count, ultimately increasing porosity within the melt[18, 37].

3.2 Effect of Na_3AlF_6 on purification of aluminum melt

At 740 °C, experiments involving salt fluxes were conducted under various conditions, including without salt fluxes addition and with varying concentrations of Na_3AlF_6 salt fluxes. The morphologies of the aluminum ingot under different conditions are shown in Fig. 6. Without adding salt fluxes, flake-like Al_2O_3 inclusions, small chip-like Al_2O_3 inclusions, and dense pores appear in the sample. Conversely, when basic salt fluxes (NaCl and KCl) are introduced, Al_2O_3 inclusions appear as fine fragment. As the Na_3AlF_6 added increases, the number of fine fragmented Al_2O_3 inclusions gradually decreases. However, some larger block-like Al_2O_3 inclusions still exist. These block-like Al_2O_3 inclusions are partly individual particles, while others result from the aggregation of numerous fragmented Al_2O_3 inclusions.

The statistical results regarding the number and size of inclusions are illustrated in Fig. 7. A significant number of inclusions smaller than 5 μm are present when no salt fluxes are added. While, as the basic salt fluxes are added, the number of inclusions smaller than 5 μm significantly diminishes. Still, inclusions are substantially increased in the 5–20 μm range. With the introduction of Na_3AlF_6, the number of inclusions initially decreases but then increases. Notably, when adding 16wt.% Na_3AlF_6, the number of inclusions is the lowest.

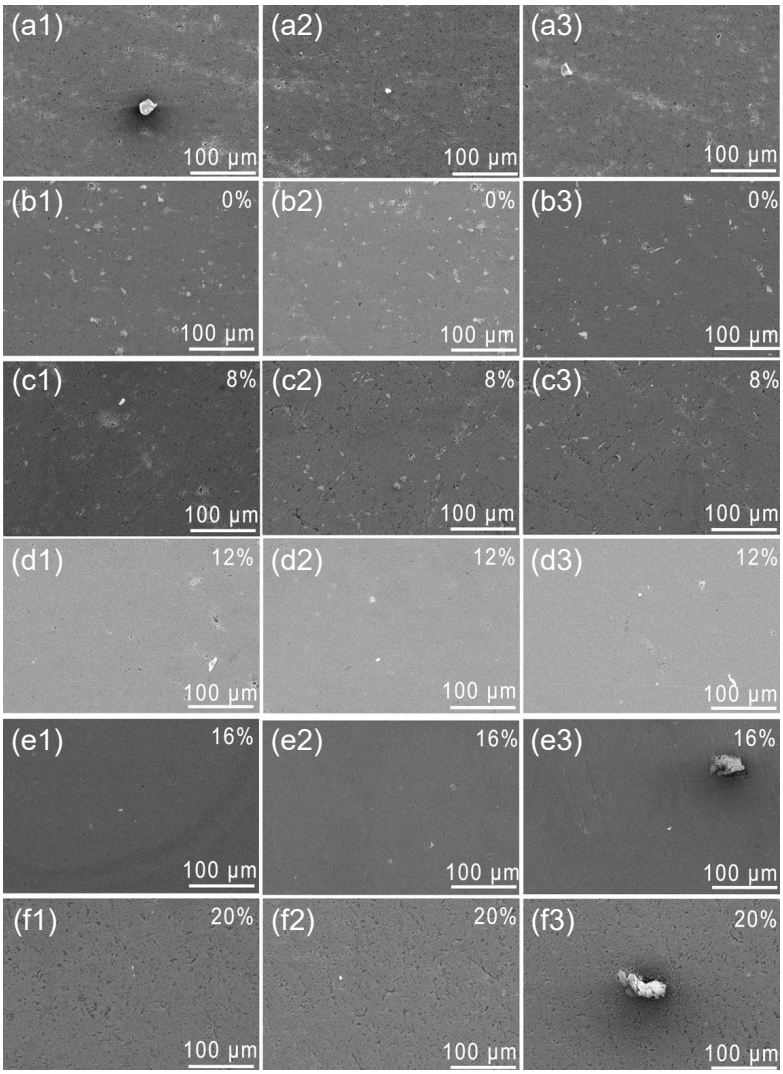

Fig. 6: Inclusion morphology under different content of Na_3AlF_6 addition: (a1–a3) without salt fluxes; (b1–b3) 0wt.% Na_3AlF_6; (c1–c3) 8wt.% Na_3AlF_6; (d1–d3) 12wt.% Na_3AlF_6; (e1–e3) 16wt.% Na_3AlF_6; (f1–f3) 20wt.% Na_3AlF_6

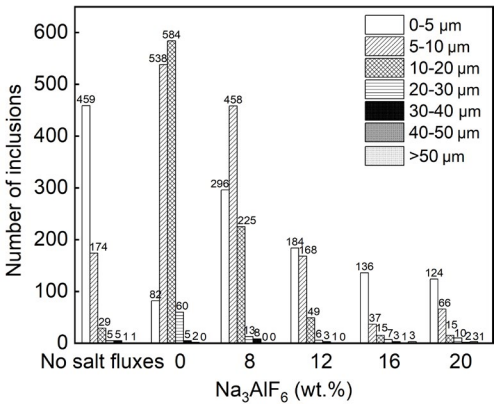

Fig. 7: Distribution of inclusion number and size under different Na_3AlF_3 addition

Without addition of salt flux, the cleanliness is relatively high, about 99.9970%. As Na_3AlF_6 added in salt fluxes increases from 0 to 20wt.%, the cleanliness increases and then slightly decreases, as shown in Fig. 8. When adding 16wt.% Na_3AlF_6, the cleanliness is the highest, about 99.9982%.

After adding salt fluxes, followed by stirring and holding, a layer of aluminum slag can form on the aluminum melt surface. The adsorption capacity of salt fluxes on aluminum oxide significantly impacts the cleanliness[10, 19, 31, 38]. The aluminum slag and residue in the crucible wall after purification with varying contents of Na_3AlF_6 was analyzed using XRD, as shown in Fig. 9. It can be seen from XRD results, aluminum slag treated by basic salt fluxes does not exhibit Al_2O_3 phase, indicating that the basic salt fluxes do not effectively transport oxide inclusions into the slag.

When Na_3AlF_6 is introduced into the salt fluxes, the α-Al_2O_3 phase appears in aluminum slag. This suggests that adding Na_3AlF_6 to salt fluxes can carry oxide inclusions from the aluminum melt to the surface. This change is beneficial for separating Al_2O_3 inclusions from the melt and purifying the aluminum melt. Figure 9(f)

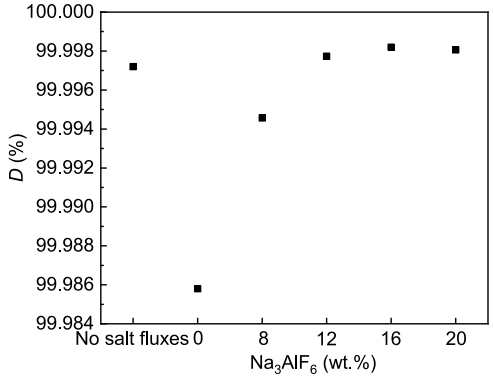

Fig. 8: Cleanliness (*D*) of aluminum melt with various Na_3AlF_3 additions

indicates that the aluminum slag treated by salt fluxes at the crucible bottom contains α-Al_2O_3 and γ-Al_2O_3. It means that γ-Al_2O_3 tends to adhere to the crucible wall and bottom instead of entering the melt.

To gain a deeper insight into the adsorption mechanism of salt fluxes on inclusions, the NaCl-KCl binary phase diagram was calculated by Factsage 7.2 software, as shown in Fig. 10. The basic salt fluxes have the lowest melting point of 657 °C, which is lower than that of pure aluminum of 660 °C. During the aluminum melting process, the basic slat fluxes form small droplets when stirring the melt, and the fluidity of the salt fluxes is enhanced.

The possible reactions between NaCl, KCl, and the aluminum melt is represented as Eqs. (3)–(4). However, thermodynamic calculations suggest that this reaction is unlikely to occur. It means that NaCl and KCl are inactive components in the salt fluxes. Their droplets can wrap, adsorb, swallow inclusions, and carry inclusions up to the surface of the melt. Then, the inclusions can be removed through skimming. However, some inclusions are not captured by salt flux droplets. They settle to the bottom of the crucible, while others are suspended in the melt, as shown in the schematic diagram in Fig. 11.

$$3NaCl+Al=AlCl_3+3Na \quad (3)$$

$$3KCl+Al=AlCl_3+3K \quad (4)$$

Furthermore, the ability of salt fluxes to remove inclusions from the aluminum melt can be determined by their wettability with oxide inclusions. The strong wettability between salt fluxes and inclusions promotes the capture, encapsulation, and swallowing of the inclusions by the salt fluxes[39]. The decrease in wettability between inclusions and aluminum melt results in the rapid removal of inclusions[18, 40, 41]. The wetting angle is a key parameter used to determine the wetting performance, as shown in Fig. 12.

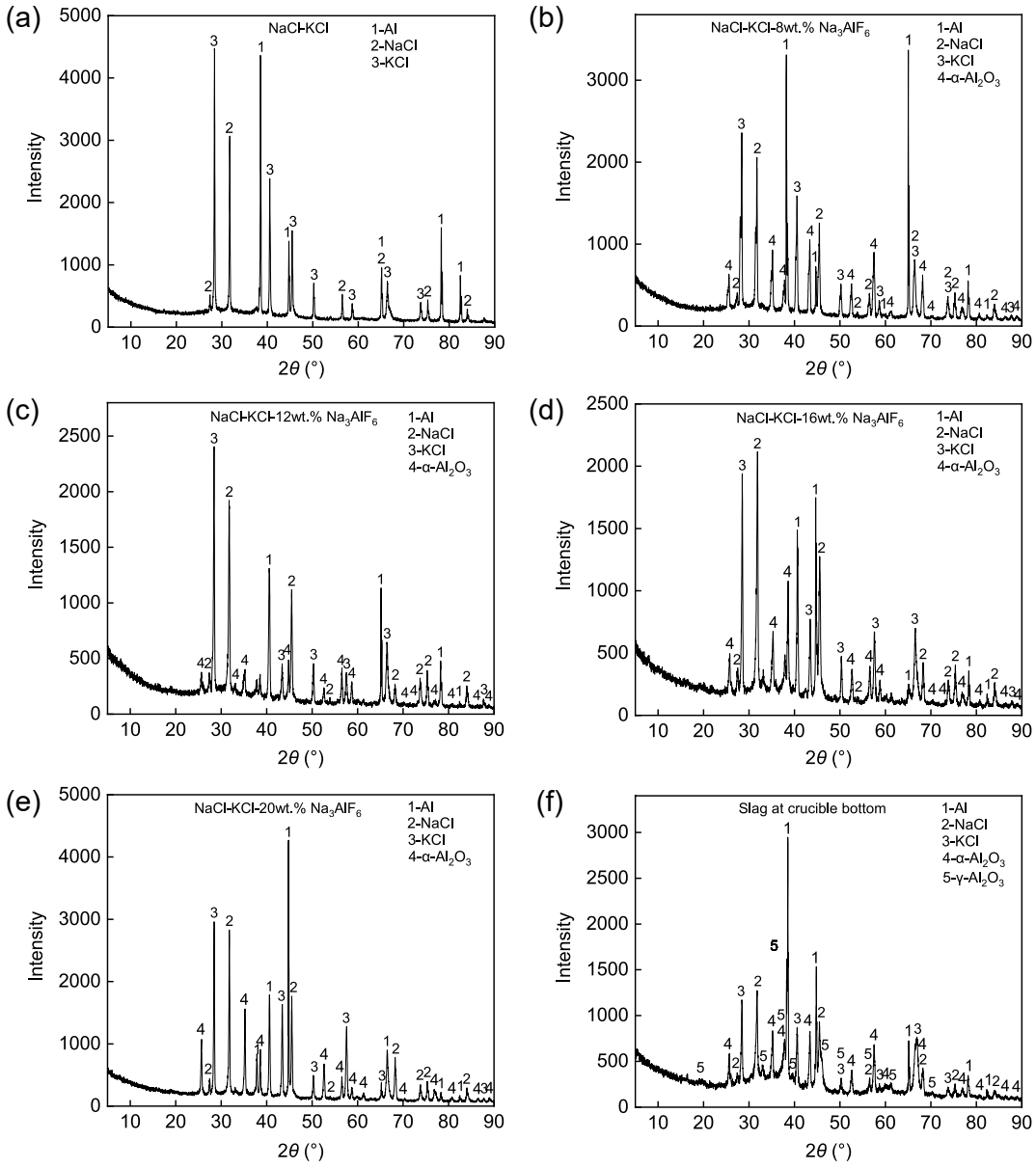

Fig. 9: Aluminum slag and residue in the crucible after purification with varying contents of Na_3AlF_6: (a) 0wt.% Na_3AlF_6; (b) 8wt.% Na_3AlF_6; (c) 12wt.% Na_3AlF_6; (d) 16wt.% Na_3AlF_6; (e) 20wt.% Na_3AlF_6; (f) slag at crucible bottom containing 12wt.% Na_3AlF_6

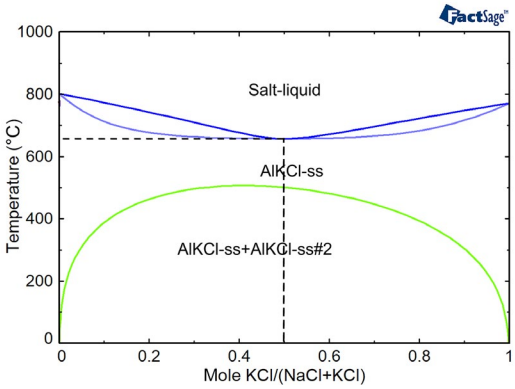

Fig. 10: KCl-NaCl binary phase diagram

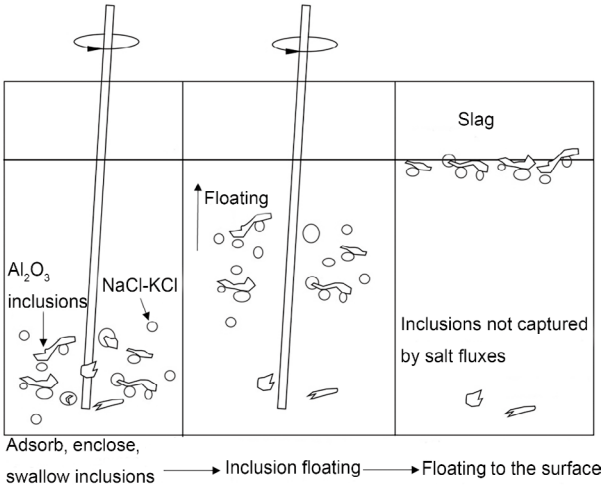

Fig. 11: Schematic diagram of basic salt fluxes refining

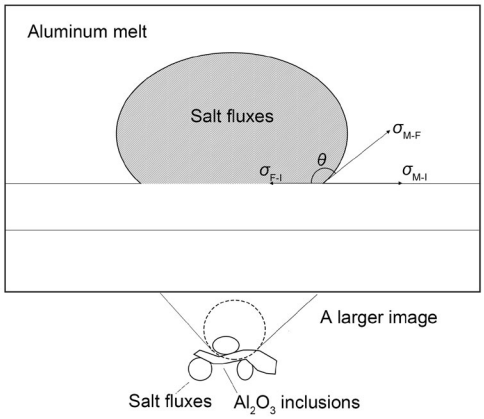

Fig. 12: Schematic diagram of wetting angle between salt fluxes and inclusion

The smaller the wetting angle, the better the wettability between salt fluxes and oxidized inclusions, leading to a stronger slag removal ability. The wetting angle (θ) is jointly determined by the interfacial tensions $\sigma_{M\text{-}F}$ (between salt fluxes and aluminum melts), $\sigma_{F\text{-}I}$ (between salt fluxes and inclusions), and $\sigma_{M\text{-}I}$ (between aluminum melt and inclusions). Their relationship is as follows:

$$\sigma_{M\text{-}I}=\sigma_{F\text{-}I}+\sigma_{M\text{-}F}\cos\theta \quad (5)$$

$$\cos\theta=\frac{\sigma_{M-I}-\sigma_{F-I}}{\sigma_{M-F}} \quad (6)$$

From Eqs. (5)–(6), it can be observed that minimizing the wetting angle requires increasing $\sigma_{M\text{-}I}$ and minimizing $\sigma_{M\text{-}F}$ and $\sigma_{F\text{-}I}$. Adding Na_3AlF_6 alters the interfacial tension between the salt fluxes, aluminum melt, and inclusions, thereby enhancing wettability. It is easier for the salt fluxes to adsorb inclusions[10, 42]. Furthermore, the addition of Na_3AlF_6 also contributes to dissolution and break up of inclusions. Al_2O_3 exhibits high solubility in Na_3AlF_6. Adding a small quantity of Na_3AlF_6 is conducive to the adsorption and dissolution of Al_2O_3 inclusions. There are four types of ions once Na_3AlF_6 is molten, as shown in Eq. (7):

$$Na_3AlF_6=3Na^{+}+(1-\alpha)\,AlF_6^{3-}+2\alpha F^{-}+\alpha AlF^{4-} \quad (7)$$

where, α is decomposition rate of AlF_6^{3-} [10]. AlF_6^{3-} reacts with Al_2O_3 as follows[43]:

$$4AlF_6^{3-}+Al_2O_3=3AlOF_5^{4-}+3AlF_3 \quad (8)$$

$$2AlF_6^{3-}+Al_2O_3=3AlOF_3^{2-}+3AlF_3 \quad (9)$$

$$4AlF_6^{3-}+Al_2O_3=3Al_2OF_8^{4-} \quad (10)$$

It is evident that AlF_6^{3-} can react with Al_2O_3 through various pathways[44]. Al_2O_3 inclusions can effectively dissolve or fragment. The smaller inclusions will form and more easily be adhered to and taken to the melt surface by salt fluxes. Simultaneously, this process facilitates the encapsulation of aluminum droplets, resulting in the amalgamation of larger aluminum droplets, which reduces aluminum loss in the aluminum melt. This transformation can also explain the change of aluminum slag from solid blocks (aluminum and slag cannot be effectively separated) to powdery dry slag (ellipsoidal aluminum droplets and slag separation) after adding Na_3AlF_6. However, the amount of Na_3AlF_6 added should not be excessive. An excessive amount can increase the viscosity of salt fluxes[39]. The high viscosity hinders the upward movement of salt fluxes and decreases the purification effectiveness.

3.3 Effect of $CaCO_3$ on purification of aluminum melt

Purification experiments were conducted with 16wt.% Na_3AlF_6 and different content of $CaCO_3$ added to the basic salt flux at melting temperature of 740 °C. As shown in Fig. 13, in the samples with 0wt.% $CaCO_3$ and 2wt.% $CaCO_3$ addition, the Al_2O_3 inclusions are mainly present as small fragments. As the content of $CaCO_3$ increases, the number of granular Al_2O_3 inclusions and black dense small pores increases. Larger inclusions are also accompanied by larger pores, as shown in Fig. 13(d1). When adding 8wt.% $CaCO_3$, small and fragmented Al_2O_3 inclusions have become denser, accompanied by small black pores, and granular Al_2O_3 inclusions further increase.

The statistical results of inclusion distribution are depicted in Fig. 14. In comparison to the sample with 0wt.% $CaCO_3$ added, the samples containing $CaCO_3$ exhibit an increase in small-sized inclusions below 5 μm. However, after adding 2wt.% $CaCO_3$, the number of inclusions larger than 10 μm decreases. As the content of $CaCO_3$ addition increases, the proportion of Al_2O_3 inclusions also increases, leading to a

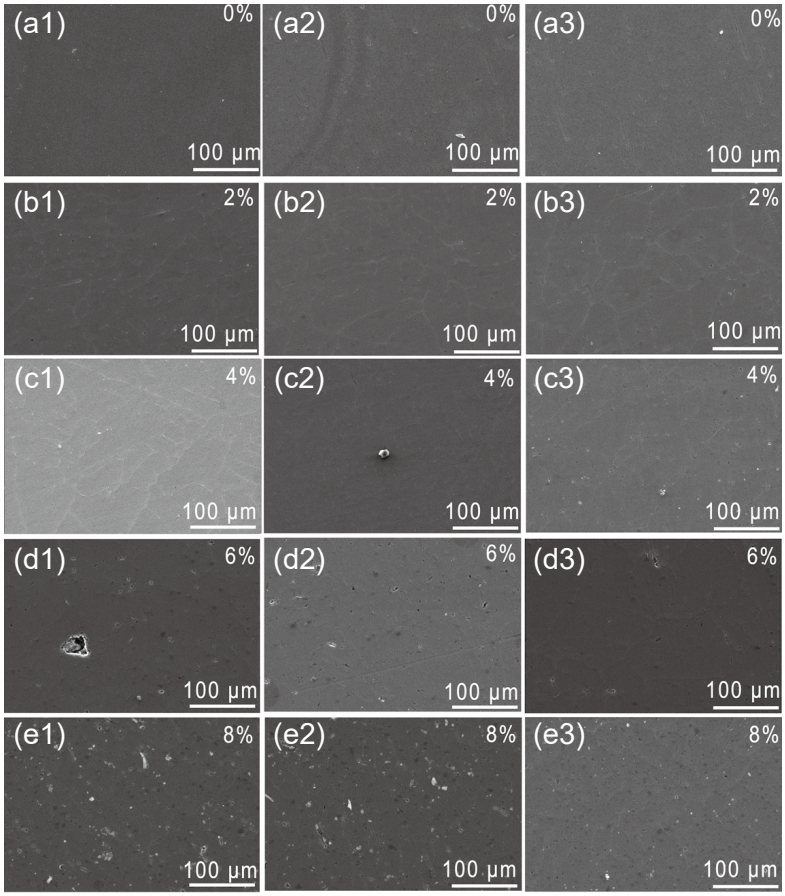

Fig. 13: Inclusion morphology under different content of $CaCO_3$ addition: (a1–a3) 0wt.% $CaCO_3$; (b1–b3) 2wt.% $CaCO_3$; (c1–c3) 4wt.% $CaCO_3$; (d1–d3) 6wt.% $CaCO_3$; (e1–e3) 8wt.% $CaCO_3$

gradual deterioration in the cleanliness of the aluminum melt. When the addition of $CaCO_3$ exceeds 4wt.%, the inclusions significantly increase, especially those larger than 5 μm. The addition of 2wt.% $CaCO_3$ results in the most effective purification, as shown in Fig. 15, with the highest cleanliness, approximately 99.99928%.

The promotion of purification by $CaCO_3$ can be attributed to gas refining. $CaCO_3$ undergoes an exothermic reaction at the melting temperature, as shown in Eq. (11):

$$3CaCO_3+2Al=3CaO+Al_2O_3+3CO\uparrow \quad (11)$$

The release of CO gas during this reaction contributes to gas refining by forming bubbles, which assist salt fluxes in adsorbing Al_2O_3 inclusions and transporting them to the melt's surface[41]. As part of the refining process, the rising temperature enhances the diffusion of Al_2O_3 inclusions into the salt fluxes. However, excessive $CaCO_3$ addition can lead to local overheating. The burning loss and Al_2O_3 inclusions increase. At the same time, the amount of Al_2O_3 inclusions carried by salt fluxes decreases.

XRD phase analysis was conducted on aluminum slag treated with different contents of $CaCO_3$, as shown in Fig. 16. When the addition of $CaCO_3$ is only 2wt.% and 4wt.%, the phase is α-Al_2O_3. However, by adding 6wt.% and 8wt.% $CaCO_3$, there may be a relatively low content of α-Al_2O_3, which results in failing to find obvious diffraction peaks. In Figs. 16(a), (b), and (c), $Na_{0.67}Al_6O_{9.33}$ (an aluminate mullite) is detected, which may be related to the addition of $CaCO_3$. Due to the small amount of slag generated, XRD analysis results can only confirm the presence of entrained aluminum, NaCl, and KCl in the slag, as shown in Fig. 16(d).

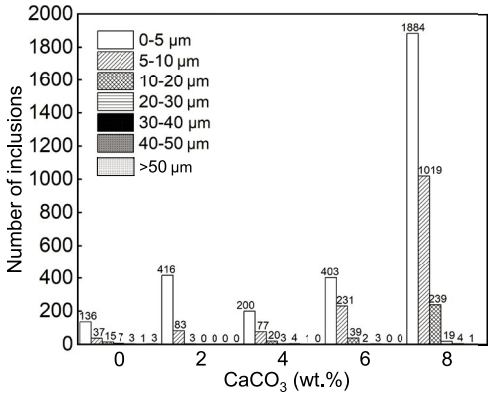

Fig. 14: Distribution of inclusion number and size with different $CaCO_3$ additions

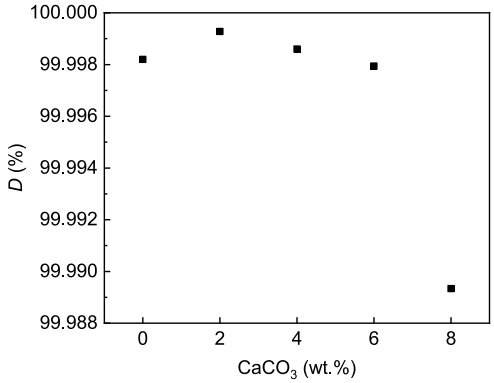

Fig. 15: Cleanliness (*D*) of aluminum melt with different $CaCO_3$ additions

3.4 Tensile properties

Research and practice have shown that inclusions in aluminum alloys can lead to metallurgical defects. Metallurgical defects directly impact alloy materials' strength, plastic deformation performance, and corrosion resistance[19, 45]. Tensile tests were conducted on samples refined with 16wt.% Na_3AlF_6 and varying amounts of $CaCO_3$, the results are shown in Fig. 17. The yield strength (YS), ultimate tensile strength (UTS), and elongation (EL) are shown in Table 2. The refined sample with a 2wt.% $CaCO_3$ addition exhibits the highest tensile properties. The increase in strength is correlated with the cleanliness of the sample. In the production of aluminum plates and foils, inclusions are known to cause holes and tears. The size and distribution of inclusions are crucial to their strength properties; small-sized precipitates and inclusions are preferable to larger ones. Such defects are less harmful within the grain structure than at the grain boundaries, where they can affect two or three adjacent grains simultaneously[46]. Therefore, the higher cleanliness which means a reduction in the number and size of inclusions, will contribute to improved performance.

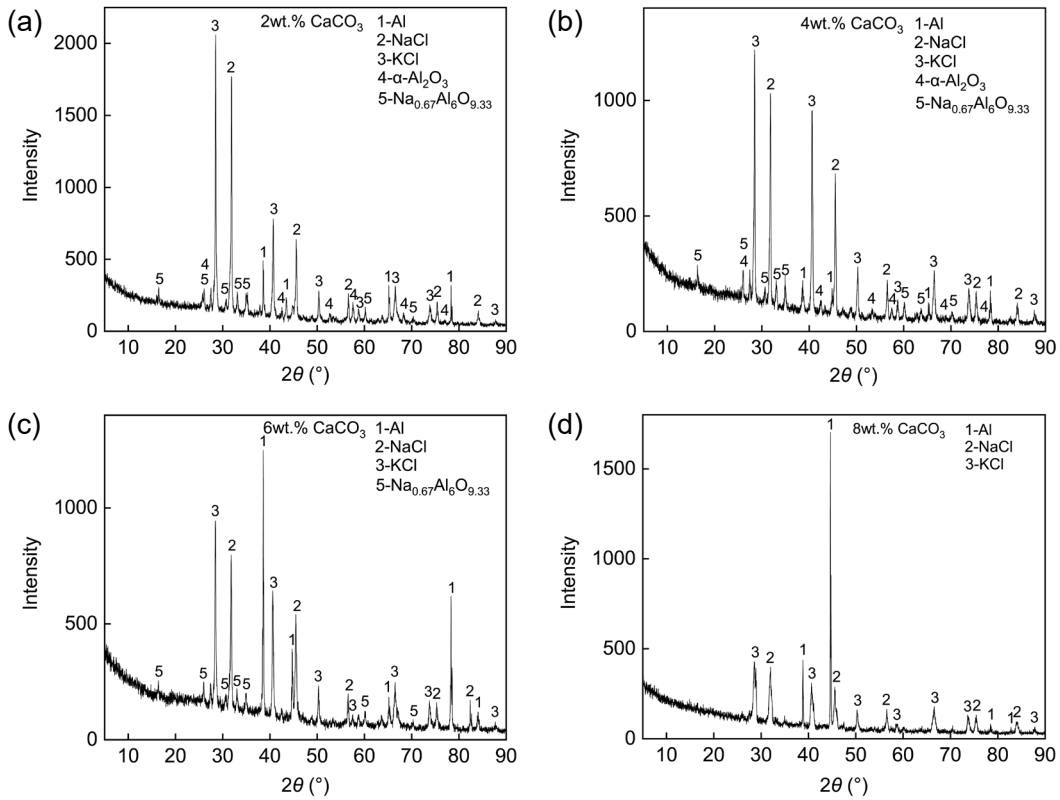

Fig. 16: Aluminum slag after purification with varying contents of $CaCO_3$: (a) 2wt.%; (b) 4wt.%; (c) 6wt.%; (d) 8wt.%

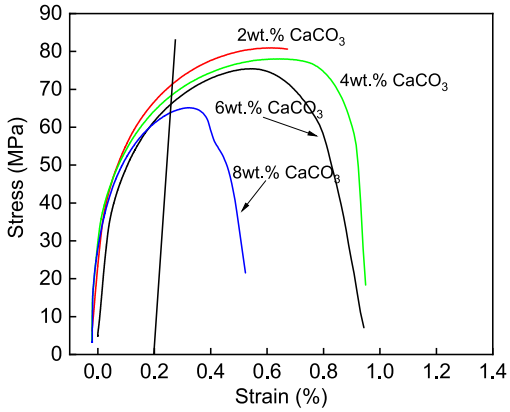

Fig. 17: Stress-strain curves of samples refined with salt fluxes containing different $CaCO_3$ contents

Table 2: Tensile properties of refined samples with different contents of $CaCO_3$ (MPa)

$CaCO_3$	YS (MPa)	UTS (MPa)	EL (%)
2wt.%	71.46±1.26	80.93±1.43	14.10±0.63
4wt.%	68.48±1.34	78.03±1.29	12.86±0.45
6wt.%	66.11±0.95	75.31±1.13	13.50±1.17
8wt.%	63.87±1.45	65.13±1.54	10.36±1.84

Additionally, inclusions and aluminum alloy matrices possess different performances, such as elastic modulus and expansion coefficient[19, 21]. Under external forces, the sharp corners of Al_2O_3 inclusions are easy to cause stress concentration, diminishing the strength and plasticity of the material and causing significant harm to the material's fatigue strength and fracture characteristics. Additionally, the hardness of Al_2O_3 inclusions significantly differs from that of aluminum alloy mixture, impeding normal flow during plastic deformation in processing and serving as a potential source of material failure, thus accelerating the fracture process of the materials[19].

4 Conclusions

In the salt fluxes purification process, the refining temperature and salt fluxes composition on the quantity and size distribution of inclusions and the mechanical properties of aluminum were investigated. The following conclusions can be drawn.

(1) Lower refining temperatures are more conducive to improving the cleanliness. As the temperature increases, the total area and the number of inclusions with sizes below 10 μm gradually increase. The degree of oxidation on the aluminum melt surface is enhanced. The γ-Al_2O_3 formed on the surface slowly transforms into α-Al_2O_3, which is more prone to fragmentation and suspension in the aluminum melt.

(2) Modified salt fluxes are effective in improving the cleanliness. In contrast, basic salt fluxes, while capable of adsorbing inclusions and floats, are difficult to separate between the melt and slag. The cleanliness is reduced, and aluminum loss is increased. Adding 16wt.% Na_3AlF_6 achieves the positive purification effect. It is related to dissolving and breaking up of Al_2O_3 inclusions and improving the separation between slag and melt.

(3) Based on a 16wt.% Na_3AlF_6 addition, the incorporation of $CaCO_3$ contributes to gas refining. Adding 2wt.% $CaCO_3$ is beneficial for the removal of inclusions. But, when the $CaCO_3$ addition exceeds 4wt.%, local overheating occurs. The number of Al_2O_3 inclusions carried by salt fluxes is reduced, and small Al_2O_3 inclusions in the melt are increased. It rapidly decreases the cleanliness of the melt.

(4) When the salt fluxes composition is 37wt.% NaCl-47wt.% KCl-16wt.% Na_3AlF_6-2wt.% $CaCO_3$, the aluminum melt achieves the highest level of cleanliness, approximately 99.99928%.

(5) The tensile properties of the aluminum samples are improved due to changes in inclusions and the enhancement of cleanliness. The yield strength, ultimate tensile strength, and elongation are highest at 71.46 MPa, 80.93 MPa, and 14.10%, respectively.

Acknowledgments

This research was supported by the National Natural Science Foundation of China (Nos. U23A20610, 52164017, 52064011, 52274331, and 521043348), the Guizhou Provincial Basic Research Program (Natural Science) (Nos. ZK [2021]258 and ZK [2023] Zhongdian 020), the Guizhou Provincial Program on Commercialization of Scientific and Technological Achievements (No. [2021]086), the Natural Science Research Project of Guizhou Provincial Department of Education (No. [2022]041), the Key Research Projects in Higher Education Institutions of Henan Province (No. 24B450003), the Zhengzhou Railway Vocational and Technical College School Scientific Research Project (No. 2024KY015), the Guizhou Province Dual-Carbon and New Energy Technology Innovation and Development Research Institute Open Project (No. DCRE-2023-01), and the Guizhou Provincial Science and Technology Projects (No. GCC[2023]017). Additionally, this project was supported by the State Key Laboratory of Advanced Metallurgy (No. K23-04).

Conflict of interest

The authors declare that they have no competing financial interests or personal relationships that could have appeared to influence the work in this paper.

References

[1] Cui Z, Li X, Xiao K, et al. Atmospheric corrosion behaviour of pure Al 1060 in tropical marine environment. Corrosion Engineering, Science and Technology, 2015, 50(6): 438–448.
[2] Telesman J, Gabb T, Kantzos P, et al. Effect of a large population of seeded alumina inclusions on crack initiation and small crack fatigue crack growth in Udimet 720 nickel-base disk superalloy. International Journal of Fatigue, 2021, 142: 105953.
[3] Bowles C, Schijve J. The role of inclusions in fatigue crack initiation in an aluminum alloy. International Journal of Fatigue, 1973, 9: 171–179.
[4] Ni H, Sun B, Jiang H, et al. Effects of rotating impeller degassing on microstructure and mechanical properties of the A356 scraps. Materials Science and Engineering: A, 2003, 352(1–2): 294–299.
[5] Espinoza-Cuadra J, García-García G, Mancha-Molinar H. Influence of defects on strength of industrial aluminum alloy Al-Si 319. Materials & Design, 2007, 28(3): 1038–1044.
[6] Gao H, Zhao B, Zhao Z, et al. A cluster of inclusions on Al-Si-Cu die casting cylinder block. Engineering Failure Analysis, 2015, 55: 370–375.
[7] Qiu C, Metselaar R. Solubility of carbon in liquid Al and stability of Al_4C_3. Journal of Alloys and Compounds, 1994, 216(1): 55–60.
[8] Pietrzyk S, Palimąka P, Gębarowski W. The effect of liquid aluminium on the corrosion of carbonaceous materials. Archives of Metallurgy and Materials, 2014, 59(2): 545–550.
[9] He Y D, Chen C, Zeng H N, et al. Process of alumina inclusion forms in electrolytic aluminum liquid with anode effect. Chinese Journal of Rare Metals, 2017, 41(1): 64–71. (In Chinese)
[10] Wan B, Li W, Liu F, et al. Determination of fluoride component in the multifunctional refining flux used for recycling aluminum scrap. Journal of Materials Research and Technology, 2020, 9(3): 3447–3459.
[11] Zhou M, Li K, Sun B, et al. A fluxing method to remove inclusions from molten aluminum. Journal of Materials Science Letters, 2002, 21: 1285–1287.
[12] Damoah L N W, Zhang L. Removal of inclusions from aluminum through filtration. Metallurgical and Materials Transactions: B, 2010, 41(4): 886–907.
[13] Wan H, Xu B, Yang B, et al. The impurities distribution and purification efficiency of high-purity aluminum preparation by zone melting in vacuum. Vacuum, 2020, 171: 108839.
[14] Wu J, Djavanroodi F, Gode C, et al. Melt refining and purification processes in Al alloys: A comprehensive study. Materials Research Express, 2022, 9(3): 032001.
[15] Zhang L, Lv X, Torgerson A, et al. Removal of impurity elements from molten aluminum: A review. Mineral Processing & Extractive Metallurgy Review, 2011, 32(3): 150–228.
[16] Cao X, Campbell J. Oxide inclusion defects in Al-Si-Mg cast alloys. Canadian Metallurgical Quarterly, 2005, 44(4): 435–448.
[17] Utigard T A. The properties and uses of fluxes in molten aluminum processing. JOM, 1998, 50(11): 38–43.
[18] Majidi O, Shabestari S G, Aboutalebi M R. Study of fluxing temperature in molten aluminum refining process. Journal of Materials Processing Technology, 2007, 182(1): 450–455.
[19] Shi M, Li Y. Performance improvement in aluminum alloy treated by salt flux with different fluorides. Journal of Materials Engineering and Performance, 2023, 32(7): 3065–3072.
[20] Tenorio J A S, Espinosa D C R. Effect of salt/oxide interaction on the process of aluminum recycling. Journal of Light Metals, 2002, 2(2): 89–93.
[21] Zhou M, Shu D, Li K, et al. Performance improvement of industrial pure aluminum treated by stirring molten fluxes. Materials Science and Engineering: A, 2003, 347(1): 280–290.
[22] Atkinson H V, Shi G. Characterization of inclusions in clean steels: A review including the statistics of extremes methods. Progress in Materials Science, 2003, 48(5): 457–520.
[23] Kundu T. Ultrasonic nondestructive evaluation: Engineering and biological material characterization. Boca Raton: CRC Press, 2003: 215–220.
[24] Hudson S W, Apelian D. Inclusion detection in molten aluminum: Current art and new avenues for in situ analysis. International Journal of Metalcasting, 2016, 10: 289–305.

[25] Silva F D A, Williams J J, Müller B R, et al. Three-dimensional microstructure visualization of porosity and Fe-rich inclusions in SiC particle-reinforced Al alloy matrix composites by X-ray synchrotron tomography. Metallurgical and Materials Transactions: A, 2010, 41: 2121–2128.
[26] Makarov S, Ludwig R, Apelian D. Electromagnetic visualization technique for non-metallic inclusions in a melt. Measurement Science and Technology, 1999, 10(11): 1047.
[27] Djurdjević M B, Odanović Z, Pavlović-Krstić J. Melt quality control at aluminum casting plants. Metallurgical & Materials Engineering, 2010, 16(1): 63–76.
[28] Enright P G, Hughes I R. A shop floor technique for quantitative measurement of molten metal cleanliness of aluminium alloys. Foundryman, 1996, 89: 390–395.
[29] Simensen C J, Strand G. Analysis of inclusions in aluminium by dissolution of the samples in hydrochloric/nitric acid. Fresenius' Zeitschrift für Analytische Chemie, 1981, 308(1): 11–16.
[30] Zedel H, Fritzsch R, Akhtar S, et al. Automated metal cleanliness analyzer (AMCA)–An alternative assessment of metal cleanliness in aluminum melts. Light Metals 2021: 50th Anniversary Edition, Springer International Publishing, 2021: 778–784.
[31] Li C, Li J G, Mao Y Z, et al. Mechanism to remove oxide inclusions from molten aluminum by solid fluxes refining method. China Foundry, 2017, 14(4): 233–243.
[32] Impey S, Stephenson D, Nicholls J. Mechanism of scale growth on liquid aluminium. Materials Science and Technology, 1988, 4(12): 1126–1132.
[33] Lee J M, Yoon J H, Kim K H, et al. Control of inclusion in aluminum alloys. Journal of Korea Foundry Society, 2003, 23(1): 15–22.
[34] Kim K. Formation of fine clusters in high-temperature oxidation of molten aluminum. Metallurgical and Materials Transactions: A, 2014, 45 (8): 3650–3660.
[35] Cai Y H, Song D F, Yang D Y, et al. Effect of Naontents in refining flux on 3D characteristics of pore and mechanical properties of recycled Al-Mg-Si alloy. Materials Today Communications, 2024, 39: 108797.
[36] Yu C L, Shen Q, Jiang H T, et al. Transformation and morphology of the surface oxides during high-temperature oxidation of aluminium. Journal of Synthetic Crystals, 2010, 39(5): 1308-1312, 1324.
[37] Haboudou A, Peyre P, Vannes A B, et al. Reduction of porosity content generated during Nd:YAG laser welding of A356 and AA5083 aluminium alloys. Materials Science and Engineering: A, 2003, 363 (1): 40–52.
[38] Gaustad G, Olivetti E, Kirchain R. Improving aluminum recycling: A survey of sorting and impurity removal technologies. Conservation and Recycling, 2012, 58: 79–87.
[39] Li Q, He K, Wu N, et al. Purification of aluminum melt in crucibles by bubble flotation. Procedia Manufacturing, 2019, 37: 438–442.
[40] Raabe D, Ponge D, Uggowitzer P J, et al. Making sustainable aluminum by recycling scrap: The science of “dirty” alloys. Progress in Materials Science, 2022, 128: 100947.
[41] Zhang G, Lu W, Wu X, et al. A new strategy on designing fluxes for aluminum alloy melt refinement. Materials, 2023, 16(6): 2322.
[42] Milani V, Timelli G. Solid salt fluxes for molten aluminum processing–A review. Metals, 2023, 13 (5): 832.
[43] Ueda M, Tsukamoto S, Konda S, et al. Recovery of aluminum from oxide particles in aluminum dross using AlF_3-NaF-$BaCl_2$ molten salt. Journal of Applied Electrochemistry, 2005, 35: 925–930.
[44] Lv X J, Xu Z, Li J, et al. Molecular dynamics investigation on structural and transport properties of Na_3AlF_6-Al_2O_3 molten salt. Journal of Molecular Liquids, 2016, 221: 26–32.
[45] Li X H, He L Z, Cao Y H, et al. Effects of microporosity on the tensile properties of aluminum alloy. Advanced Materials Research, 2012, 422: 627–631.
[46] Murakami Y. Material defects as the basis of fatigue design. International Journal of Fatigue, 2012, 41: 2–10.